Building Technologies & Urban Systems Division
Energy Technologies Area
Lawrence Berkeley National Laboratory

Energy flexibility quantification of a tropical net-zero office building using physically consistent neural network-based model predictive control

Wei Liang[1] [2], Han Li[2], Sicheng Zhan[3], Adrian Chong[3], Tianzhen Hong[2]

[1]School of Architecture, Carnegie Mellon University, Pittsburgh, 15213, PA, USA, [2]Building Technology & Urban Systems Division, Lawrence Berkeley National Laboratory, Berkeley, 94720, CA, USA c Department of the Built Environment, [3]National University of Singapore, 117566, Singapore

Energy Technologies Area
July 2024

doi.org/10.1016/j.adapen.2024.100167

This work was supported by the Assistant Secretary for Energy Efficiency and Renewable Energy, Building Technologies Office, of the US Department of Energy under Contract No. DE-AC02-05CH11231.

Disclaimer:

Advances in Applied Energy 14 (2024) 100167

Contents lists available at ScienceDirect

Advances in Applied Energy

journal homepage: www.elsevier.com/locate/adapen

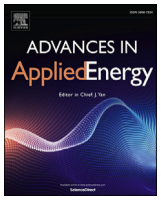

Energy flexibility quantification of a tropical net-zero office building using physically consistent neural network-based model predictive control

Wei Liang [a,b], Han Li [b], Sicheng Zhan [c], Adrian Chong [c], Tianzhen Hong [b,*]

[a] School of Architecture, Carnegie Mellon University, Pittsburgh, 15213, PA, USA
[b] Building Technology & Urban Systems Division, Lawrence Berkeley National Laboratory, Berkeley, 94720, CA, USA
[c] Department of the Built Environment, National University of Singapore, 117566, Singapore

ARTICLE INFO

Keywords:
Grid-interactive efficient buildings
Energy flexibility
PV and BESS
Model predictive control (MPC)
Physics-informed neural network (PINN)

ABSTRACT

Building energy flexibility plays a critical role in demand-side management for reducing utility costs for building owners and sustainable, reliable, and smart grids. Realizing building energy flexibility in tropical regions requires solar photovoltaics and energy storage systems. However, quantifying the energy flexibility of buildings utilizing such technologies in tropical regions has yet to be explored, and a robust control sequence is needed for this scenario. Hence, this work presents a case study to evaluate the building energy flexibility controls and operations of a net-zero energy office building in Singapore. The case study utilizes a data-driven energy flexibility quantification workflow and employs a novel data-driven model predictive control (MPC) framework based on the physically consistent neural network (PCNN) model to optimize the building energy flexibility. To the best of our knowledge, this is the first instance that PCNN is applied to a mathematical MPC setting, and the stability of the system is formally proved. Three scenarios are evaluated and compared: the default regulated flat tariff, a real-time pricing mechanism, and an on-site battery energy storage system (BESS). Our findings indicate that incorporating real-time pricing into the MPC framework could be more beneficial to leverage building energy flexibility for control decisions than the flat-rate approach. Moreover, adding BESS to the on-site PV generation improved the building self-sufficiency and the PV self-consumption by 17% and 20%, respectively. This integration also addresses model mismatch issues within the MPC framework, thus ensuring a more reliable local energy supply. Future research can leverage the proposed PCNN-MPC framework for different data-driven energy flexibility quantification types.

1. Introduction

Driven by global commitments to decarbonization goals and the imperative to address climate change, the penetration of renewable energy resources into conventional fossil fuel-based electricity generation systems is increasing. Fossil fuel is still dominant in the energy supply of countries in tropical regions. It would be beneficial for tropical countries to exploit renewable energy resources. For instance, Singapore, the city-state, acutely vulnerable to climate change impacts [1], leans heavily on gas and oil for its power needs [2], with renewables accounting for merely 1% of the nation's total energy consumption [3] in 2020.

However, the availability of different renewable energy resources varies vastly in tropical regions. For example, Singapore has very limited alternative renewable resources other than solar photovoltaics (PV) [3–5]. Solar PV is the most promising renewable energy source in tropical countries, given the high solar power potential in the region. However, due to spatial limitations, PV installations remain constrained to rooftops and certain lands, restricting their potential contribution to island and peninsula countries in tropical regions. The roadmap toward decarbonization targets in the tropics must prominently incorporate technical flexibility resources such as smart grids, distributed energy resources (DER), and energy storage systems (ESS). Among the advanced technical solutions, ESS is identified as a pivotal tool to mitigate solar intermittency and reserve energy for a reliable and resilient grid.

Another indispensable approach for topical regions' sustainability goals is enhancing building energy flexibility. Buildings are responsible for more than 55% of electricity energy consumption globally [6]. Building energy flexibility is essential for providing an efficient and resilient grid as it evaluates the building's capability to manage energy

* Corresponding author.
E-mail address: thong@lbl.gov (T. Hong).

https://doi.org/10.1016/j.adapen.2024.100167
Received 13 November 2023; Received in revised form 18 February 2024; Accepted 18 February 2024
Available online 24 February 2024

Nomenclature

Abbreviation

BESS	Battery energy storage systems
DDP	Demand decrease percentage (%)
EDP	Energy decrease percentage (%)
EF	Energy flexibility
NEMS	National electricity market of Singapore
PCNN	Physically consistent neural network
PINN	Physics-informed neural network
PV	Photovoltaics
RTP	Real-time price
SC	Self-consumption (%)
SQP	Sequential quadratic programming
SS	Self-sufficiency (%)
ToU	Time-of-use
USEP	Uniform Singapore energy price
WEP	Wholesale energy price

Symbol

η	Battery efficiency
D	Black-box module
E	Physically-consistent module
G	Global horizontal irradiance
N	Prediction horizon
T	Temperature (°C)
U, u	HVAC thermal energy input (kW)
SoC	State of charge (%)

Superscript and Subscript

$neigh$	Adjacent thermal zones
NN	Neural network
OA	Outdoor air
ref	Reference signal
SA	Supply air

demand in response to various conditions. Yet, common strategies to achieve energy flexibility include pre-cooling, which may not apply to buildings in tropical regions as they have a light thermal mass. As a result, solar PV and Building Energy Storage Systems (BESS) present potent avenues to achieve desired energy flexibility. However, quantifying the energy flexibility of buildings utilizing building-level PV and BESS applications in tropical regions has been underexplored. Furthermore, a robust control strategy is required to realize the potential of building-level PV and BESS. To address these research gaps, we presented a case study that uses a data-driven energy flexibility quantification framework to develop a novel model predictive control (MPC) framework to optimize the energy flexibility of a tropical building. The novelty and contributions of this study are as follows:

- The study investigates the impact of different electricity pricing mechanisms on energy flexible control decisions for a tropical building and the improvement to load matching between local consumption and PV generation by integrating a BESS.
- The control-oriented data-driven model in the MPC framework is developed based on the recently proposed physically consistent neural network (PCNN) model to optimize the building energy flexibility. To the best of our knowledge, this is the first instance where PCNN is applied to a mathematical MPC setting.
- The proposed PCNN-MPC framework is demonstrated on a real-world dataset of a net-zero-energy office building in Singapore through numerical simulations, and its stability is formally proved.

The rest of this paper is outlined as follows. Section 2 illustrates the background of this research from different dimensions - energy flexibility of tropical buildings, electricity price scenarios in Singapore, and control-oriented physics-informed neural networks (PINN), with a particular emphasis on physics-consistent neural networks (PCNN). Section 3 illustrates the data-driven energy flexibility quantification workflow that applies to this study, and section 3.2 elaborates on the modeling and control formulation in detail. Section 4 displays numerical simulation results. Section 5 discusses key findings and takeaways, limitations of the existing study, and future research opportunities. Section 6 draws conclusions.

2. Related work

This section presents this study's background knowledge and literature review.

2.1. Energy flexibility of buildings in tropical regions

The International Energy Agency's (IEA) Energy in Buildings and Communities Programmes (EBC) defines energy flexibility (EF) as *"a building's ability to manage its demand and generation according to local climate conditions, user needs, and energy network requirements"* [7]. It also introduced different strategies for building energy flexibility, including building mass, BESS, fuel switch, and on-site generation [8]. Both commercial [9] and residential [10] buildings show their energy flexibility potential for grid interaction.

Energy flexibility quantification is essentially about the process of deriving quantitative metrics to evaluate the energy flexibility potential in existing conditions and with certain design or operational strategies. Recently researchers have investigated methods to standardize and facilitate energy flexibility quantification with semantic ontologies [11] and define and calculate key performance indicators (KPIs) that support the assessment [12,13].

Although abundant studies have delved into building energy flexibility and energy flexibility quantification based on previous literature reviews [12,10], explorations remain limited for buildings in tropical regions. One of the reasons is that it is difficult to tackle thermal mass in tropical buildings. Exploiting thermal mass is one of the most common strategies to achieve energy flexibility. The thermal mass of a building allows for pre-conditioning indoor environments and shifting the demand for the building heating, ventilation, and air conditioning (HVAC) systems. In fact, buildings in tropical regions are constructed with relatively light thermal mass [14,15]. Therefore, the potential of demand reduction using pre-conditioning is limited for tropical buildings in simulation studies, resulting in marginal reductions in electricity costs [16,17].

Other strategies are needed to increase the energy flexibility of buildings in the tropics, such as emerging distributed energy resources (DER), including on-site power generation and behind-meter battery energy storage systems (BESS) [11]. Singapore is a suitable example in this regard. Given the nation's abundant solar penetration levels, solar PV is the most promising on-site renewable generation. However, the growth of solar PV energy generation might lead to a generation-load imbalance, known as the duck curve, which might impose a risk on the operation of current fossil-fueled electricity generation in Singapore. One approach to addressing this problem is to improve the self-consumption [18] of locally connected PV power. Hanif et al. [19] proposed a cost-optimal operation strategy for an energy-flexible building to reduce the reverse power flow, namely the excess PV output fed to the grid, of on-site solar PV generation. Zhan et al. [20] introduced a practical optimal control framework targeting the energy flexibility

of an office building in Singapore to enhance the local consumption of PV-generated power. Their method improved the PV self-consumption and building self-sufficiency by 19.5% and 10.6%, respectively, relative to baseline control. Moreover, a viable approach to boost PV self-consumption involves storing the excessive generation using BESS and exploiting it when PV generation decreases. Yet, given Singapore's flat electric tariff, BESS may not be favorable to building owners and stakeholders. Comodi et al. [21] conducted a techno-economic analysis of different energy storage systems under different tariff scenarios in Singapore. Their findings indicate that as the discrepancy between off-peak and peak electricity rates widens, the annual savings attributed to BESS increase. To harness the full potential of energy flexibility in Singaporean buildings equipped with solar PV and BESS, flexible tariff plans that acknowledge these technological advancements are imperative.

2.2. Electricity tariff mechanisms in Singapore

Singapore has taken progressive steps towards the liberalization and reconstruction of the national electricity market. Commenced in 2003, the National Electricity Market of Singapore (NEMS), supervised by the Energy Market Authority (EMA), paves the road of commercialized supply in the nation's electricity market [22]. NEMS consists of a wholesale market and a retail market. In the wholesale market, buyers (retailers and qualified consumers) and sellers (generators, qualified prosumers) trade energy through a dynamic price, the Uniform Singapore Energy Price (USEP), which varies every half an hour based on real-time settlements. In the retail market, consumers over 20,000 kWh are allowed to choose retailers according to their electricity needs. In 2018, the government established the Open Electricity Market (OEM), allowing all Singapore consumers, regardless of their demand capacity, be able to choose their own electricity retailers.

After the full liberalization of the electricity market in Singapore, dynamic pricing, such as time-of-use (ToU) and real-time prices (RTP), were introduced to the city-state's electricity market. Consumers in Singapore now have three options to purchase electricity: 1) A regulated flat-rate tariff that varies quarterly from the state-owned supplier. 2) An electricity plan from a retailer participating in the OEM. As the market is competitively priced, retailers offer diverse plans, such as flat rates, time-of-use (ToU) prices, and real-time prices (RTP). 3) Purchase electricity with the wholesale electricity price (WEP), which follows the identical fluctuation pattern of USEP every half an hour.

Dynamic pricing has been proven to promote renewable energy and energy storage investment at both utility [23–25] and district level [26,27]. Moreover, dynamic pricing can incentivize building energy flexibility, such as load shedding and load shifting [28], minimize the energy purchased from the grid, and maximize self-consumption for buildings equipped with on-site renewable energy [29]. As a country embracing renewable energy and energy storage, more and more varieties of dynamic electricity pricing can benefit the utility, retailers, and customers in the foreseeable future. This paper discusses and incorporates two pricing options into the case study: the regulated flat rate tariff provided by the state-owned supplier and a dynamic pricing scenario using WEP.

2.3. Control-oriented physics-informed neural networks

Modern buildings have offered tremendous data in recent years with the popularization of building automation systems (BAS) and the Internet of Things (IoT). This surge has stimulated the exploration of machine learning (ML) methodologies applied to the modeling of building thermal dynamics and the formulation of energy-efficient and energy-flexible control algorithms. However, it is important to note that despite the ascendancy of ML methodologies, the field of building energy modeling and controls remains deeply rooted in well-established physical principles, including thermodynamics and heat transfer, that humans have long comprehended.

While ML methods achieve state-of-the-art accuracy, there is no guarantee that the models obey the underlying physical principles, leading to potential pitfalls in interpretability and validity. For example, Di Natalie et al. [30] compared the predictive capabilities of the indoor air temperature using a physics-driven Resistance-Capacitor (RC) thermal model against a conventional ML model, the Long Short-Term Memory network (LSTM). Despite LSTM's remarkable performance in the training and validation phases, it exhibited shortcomings in capturing the nuances of heating and cooling power input levels.

Incorporating physical principles and constraints into machine learning methodologies not only enhances their accountability but also significantly improves their interpretability. Using interpretable machine learning algorithms provides potential benefits for energy flexibility quantification, as they can develop more explainable and efficient energy management strategies and help building managers make informed and understandable decisions [31].

As one of the interpretable machine learning methods, proposed physics-informed neural networks (PINN) draw attention from the building energy management research community. PINN aims to ensure that the model can be easily understandable, interpretable, and implementable. Most PINN frameworks for building thermal modeling are considered control-oriented models [32,33,30,34]. Depending on how these constraints are incorporated, several variants or types of PINN methods have emerged:

- Loss Function Augmentation: [33,35]: This is considered the classical PINN framework, which was first utilized to solve nonlinear partial differential equations [36] (PDEs). In the realm of building thermal modeling, loss function augmentation within PINNs introduces physical insights into regularization terms during model training. In practice, this framework extends to building energy modeling, with the loss function incorporating latent states derived from physics-driven RC models, thereby steering the model toward a physically meaningful space. This approach finds application in the evaluation of building energy flexibility [35].
- Physical-based model identification with Neural Networks [32]: Parameter identification of building system models is a difficult and complex task [37]. For example, a multi-zone thermal model can be simplified as a first-order linear time-invariant (LTI) multiple-input multiple-output (MIMO) system:

$$\mathbf{T}_{k+1} = \mathbf{A}\mathbf{T}_k + \mathbf{B}\mathbf{U}_k + f_d(\mathbf{d}_k) \tag{1}$$

  where $\mathbf{T}_k$ represents the values of the states (including observable states such as room temperatures and hidden states such as building envelope temperatures), $\mathbf{U}_k$ represents building HVAC inputs, and $f_d(\mathbf{d}_k)$ represents disturbances, usually introduced by outdoor air temperature, solar irradiance, and occupancy behaviors. The disturbance function $f_d(\mathbf{d}_k)$ is usually simplified as a linear function or attributed as an error term. Conventional approaches for the identification of the aforementioned systems are to find matrices $\mathbf{A}$, $\mathbf{B}$, $\mathbf{C}$ using data-driven methods like prediction error methods and subspace methods [37]. Drogňa et al. [32] proposed a PINN framework that replaces the components in Equation (1) with decoupled deep neural networks. The proposed PINN framework improved significantly in terms of mean squared error (MSE) compared to the classical linear system identification methods.
- Neural Network Architecture Alteration [34]: Rather than replacing physical components within traditional physics-based models with neural network blocks, this framework leverages the inherent structure of neural networks to enforce adherence to physical constraints. The advantage of directly altering the NN's architecture is that the underlying physical laws can be enforced by design, i.e., at all times. For instance, Wang et al. [34] proposed a partially connected neural network, forcing the prediction of each time step

only receives information from historical and current time steps. The proposed model is a surrogate of an extended state space model over a certain prediction horizon.

Another approach that alters NN's architecture is concurrent NN and physics-based model structure [30,38]. The recently proposed physically consistent neural network (PCNN) model combined a physics-based linear model running in parallel to a classical NN. The linear model ensures the physics consistency with respect to control inputs to ensure that turning the cooling on at previous timesteps leads to lower zone temperatures at the present timestep.

PINN has been widely used in two model-based control approaches, model predictive control (MPC) and model-based reinforcement learning (RL) [39]. In Model-Based Reinforcement Learning (MBRL), an agent engages with its environment to gain understanding and subsequently constructs a model of this environment through interaction. Compared to Model-Free Reinforcement Learning (MFRL), MBRL exhibits superior data efficiency and quicker convergence. Nevertheless, a fundamental challenge in MBRL is to develop an accurate and feasible model. PINN models are advantageous in this context due to their state-of-the-art accuracy and simpler implementation relative to pure deep learning models.

On the other hand, it is worth noting that MBRL can involve online training, which can impose substantial computational costs [40,41]. In contrast to MBRL, MPC uses the model to determine the influence of future inputs on the building dynamics and solve for an optimal online solution. The formulation of the model within the context of MPC can take on various forms. As one of the data-driven approaches, PINN can be seamlessly integrated into the MPC framework and employed in the online optimal control formulation [39]. [42] applied the neural network state space model (NN-SSM) into a proposed differentiable predictive control (DPP) framework. The DPP framework resembles the control optimization in the MPC framework by conducting backward propagation and forward propagation. Similarly, Chen et al. [35] harnessed a PINN model augmented with a specialized loss function for MPC, aiming to explore demand response potentials within a controlled environment chamber. Meanwhile, Wang et al. [34] introduced a masked neural network that ensures temporal correlations between inputs and outputs, seamlessly integrated into a hierarchical data-driven MPC framework (HDDPC). Notably, this model facilitated predictions for indoor temperature and CO_2 dynamics, and the ensuing HDDPC framework optimized energy consumption at both room and system levels, achieving significant reductions of 35% in system cooling load and 70% in airside coil load during a month-long simulation.

The literature reviewed above underscores the promising efficacy of PCNN within the MPC framework. Another control-orientated physics-informed machine learning model, PCNN [30,38], consists of an NN model predicting free-floating thermal dynamics and an RC-inspired physics-based model predicting energy accumulation and heat transfer in the building. Notably, the amalgamation of predictions from these two components has demonstrated better performance compared to conventional RC models.

2.4. Research gaps

From a systematic review of energy flexibility in tropical regions, the practical status quo in electricity pricing in Singapore, and existing PINN models and controls, we identify the following research gaps:

- The studies on energy flexibility quantification for tropical buildings are limited, especially for buildings with emerging DERs, such as on-site renewable and BESS.
- Given the predominance of regulated flat-rate electricity pricing in Singapore, there is a pressing need to explore dynamic pricing options to enhance energy flexibility in buildings.
- The recently proposed PCNN model has not been integrated into an MPC framework despite the inherent control-oriented modularity of its neural network and physics-based segments. This modularity suggests that it is feasible to devise an MPC formulation that leverages the strengths of both components.

Therefore, we demonstrate a building energy quantification workflow for a net-zero tropical office building. The study investigates the potential of a dynamic pricing mechanism for a net-zero office building in Singapore, providing insights for policy-makers and building owners for informed decision-making processes. To support the energy flexibility quantification, we develop a novel MPC framework that implements the PCNN model mathematically to optimize the building energy flexibility with proven stability.

3. Methodology

This case study was developed based on a recently proposed data-driven framework for quantifying energy flexibility in buildings [43]. The workflow is as follows:

- **Determine application type**: This study investigates the potential for building energy flexibility within a tropical net-zero-energy office building. We evaluate various scenarios, each characterized by distinct portfolios of electricity tariffs and differing conditions regarding the presence or absence of a BESS. Therefore, this work may be attributed as prospective, considering various electricity tariff schemes and BESS configurations.
- **Select KPIs:**: To demonstrate the quantification of load shedding, two baseline-required KPIs are selected: the demand decrease percentage (DDP) and energy decrease percentage (EDP). They can be used to quantify the effectiveness of the proposed control strategy to manage energy consumption during peak periods. Additionally, the building energy flexibility was reflected in the consumption of PV generation and the assistance of BESS. As a result, two on-site generation-related KPIs, such as self-consumption [18] and self-sufficiency [44]. The formula and terms the four selected energy flexibility quantification KPIs are listed in Table 1 below.
- **Understand KPI Inputs**: It is observed from Table 1 that the two load shedding related KPIs both require a baseline and a proposed flexible electric load profile as the inputs. The start time and the duration of the load shedding period also need to be specified. In addition, two on-site generation related KPIs require the total PV generation, the PV generation that charges the BESS, and the PV generation that is directly consumed by the load under both baseline and proposed flexible scenarios.
- **Determine data-driven modeling methods**: This case study requires a counterfactual load profile of the future flexible operation scenario under the MPC strategy and with a virtual BESS compared to the baseline load profile. Control-oriented modeling techniques are crucial for a practical data-driven MPC framework. While there is a wide range of control-oriented models for building dynamics, the recently proposed PCNN model family shows state-of-the-art accuracy in previous case studies [38,45] and consistent compliance to the underlying physics by design. Given the complexity of the testbed as a net zero energy and naturally ventilated building, the S-PCNN model was selected. The model comprises two modules: an NN model predicting free-floating thermal dynamics with variables that are difficult to build physics-based models with, such as CO_2 concentration, plug and ceiling fan electricity loads, and solar irradiance, and an RC-inspired physics-based model predicting energy accumulation and heat transfer in the building with the HVAC input, outdoor air temperature, and temperatures of thermal zones in the testbed.

Table 1
Four energy flexibility KPIs used in the case study.

Metrics	Formula	Terms
Demand Decrease Percentage (DDP)	$DDP(\%) = \frac{P_{load,shed}}{P_{ref,load}} \times 100\%$	$P_{ref,load}$ is the baseline peak power demand; $P_{load,shed}$ is the peak power demand shedded
Energy Decrease Percentage (EDP)	$EDP(\%) = \frac{E_{load,shed}}{E_{ref,load}} \times 100\%$	$E_{ref,load}$ is the baseline daily energy consumption; $E_{load,shed}$ is the daily energy consumption shed
self-consumption (SC)	$SC = \frac{E_{PV,load}+E_{PV,charge}}{E_{PV}} \times 100\%$	$E_{PV,load}$ is the part of PV generation that is directly consumed on-site; $E_{PV,charge}$ is the part of PV generation that directly charges the BESS; E_{PV} is the daily accumulated PV generation
self-sufficiency (SS)	$SS = \frac{E_{PV,load}}{E_{load}} \times 100\%$	$E_{PV,load}$ is the part of PV generation that is directly consumed on-site; E_{load} is the daily total energy consumption

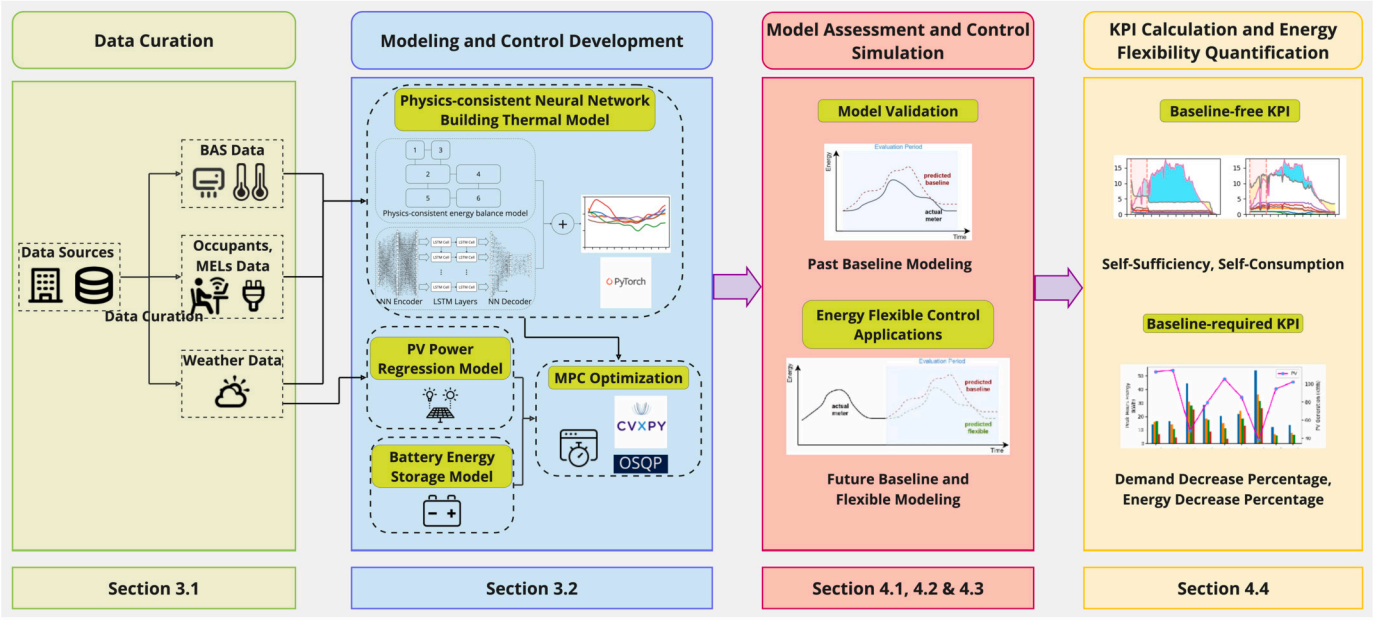

Fig. 1. Data-driven energy flexibility (EF) quantification roadmap for the case study. The mapping to section numbers is shown at the bottom.

The remaining three steps of the data-driven energy flexibility quantification framework, *Curate Data*, *Develop model and simulation* and *Calculate KPIs*, are illustrated in the framework diagram of this work in Fig. 1.

3.1. Data curation

The data used in the study was collected from a newly built net zero energy building in Singapore. The building has an on-site PV generation system on the rooftop that generates electricity of around the same amount as the building consumes in a year.

The virtual testbed consists of six-zone office spaces - four offices and two conference rooms, served by two dedicated outdoor air systems (DOAS) associated with variable air volumes (VAV). Ceiling fans were installed in each room and controlled by occupants as part of the hybrid cooling system. The data points collected can be found in [20] and are categorized based on an extended Level of Detail (LoD) framework in [46].

In addition to the building characteristics and sensor and meter data, the RTP of the electricity consumption in Singapore, namely the half-hourly wholesale electricity prices (WEP), can be accessed online [47].

Lastly, the virtual BESS is sized to cover the peak PV electric power generation. The parameters of the BESS, such as the discharging/charging efficiency, maximum charging/discharging rate, and maximum and minimum state of charge, are specified with real-world products.

3.2. PCNN-MPC framework

In this section, we present the PCNN-MPC framework that serves as the data-driven model to calculate energy flexibility KPIs. Details of different prospect modeling scenarios, namely flat-rate tariff scenario, dynamic pricing scenario, and dynamic pricing scenario with BESS, are illustrated with details.

3.2.1. S-PCNN modeling

We adopted the S-PCNN model from [38] to model the thermal dynamics of multi-zone buildings. The diagram of S-PCNN in detail is shown in Fig. 2. In this network, all zones share the same black-box and physics-inspired modules. As a result, we can represent the architecture as a state-space model:

$$\boldsymbol{D}_{k+1} = \boldsymbol{D}_k + f_{\boldsymbol{NN}}(\boldsymbol{x}_k) \tag{2}$$

$$\boldsymbol{E}_{k+1} = \boldsymbol{E}_k + \boldsymbol{a} \odot \boldsymbol{u}_k - \boldsymbol{b} \odot (\boldsymbol{T}_k - \boldsymbol{T}_k^{OA}) - \boldsymbol{c} \odot (\boldsymbol{T}_k - \boldsymbol{T}_k^{neigh}) \tag{3}$$

$$\begin{aligned}\boldsymbol{T}_{k+1} &= \boldsymbol{D}_{k+1} + \boldsymbol{E}_{k+1} \\ &= \boldsymbol{T}_k + \boldsymbol{a} \odot \boldsymbol{u}_k - \boldsymbol{b} \odot (\boldsymbol{T}_k - \boldsymbol{T}_k^{OA}) - \boldsymbol{c} \odot (\boldsymbol{T}_k - \boldsymbol{T}_k^{neigh})\end{aligned} \tag{4}$$

$$\begin{aligned}\boldsymbol{D}_0 &= \boldsymbol{T}_0 \\ \boldsymbol{E}_0 &= \boldsymbol{0}\end{aligned} \tag{5}$$

In this architecture, $\boldsymbol{D}_{k+1} = \boldsymbol{D}_k + f_{\boldsymbol{NN}}(\boldsymbol{x}_k)$ represents the prediction by the black-box module, which can be any neural network. In this work, we use LSTM, given its ability to handle time-series data. The features $\boldsymbol{x}_k$ include the CO_2 concentration (which represents the occupants), plug-loads and ceiling fan electricity loads, and artificial features created from the timestamp (month, time of the day, day of the week). $\boldsymbol{E}_{k+1} = \boldsymbol{E}_k + \boldsymbol{a} \odot \boldsymbol{u}_k - \boldsymbol{b} \odot (\boldsymbol{T}_k - \boldsymbol{T}_k^{OA}) - \boldsymbol{c} \odot (\boldsymbol{T}_k - \boldsymbol{T}_k^{neigh})$ is the physically consistent term, which is inspired by the first-order RC model. Note that $\boldsymbol{u}_k$ is the HVAC input. The HVAC input is computed with the

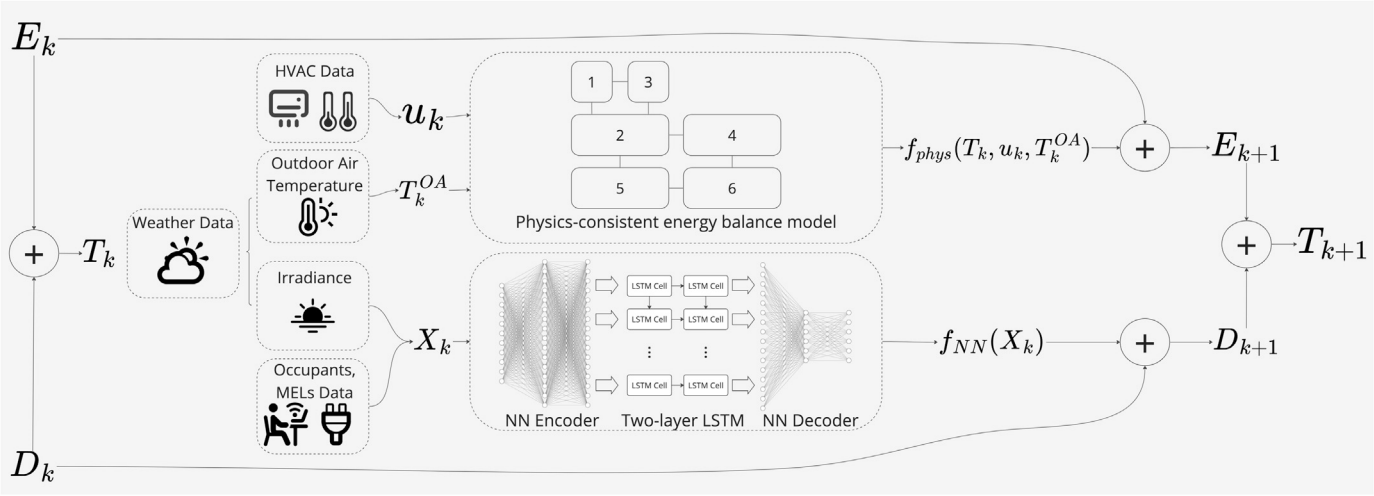

Fig. 2. A PCNN model diagram.

historical FCU data, namely the FCU supply air temperature and its affiliated VAVs airflow rates, collected in SDE4. The HVAC input function is $\boldsymbol{u}_k = c_\rho \dot{m}_k^{\text{VAV}}(\boldsymbol{T}_k^{SA} - \boldsymbol{T}_k)$, which will be used as the control variable in the PCNN-MPC framework.

Remark 3.1. (Physical Consistency of S-PCNN) Physical consistency [30] with respect to an input is defined as a change in the output caused by any changes in this input in accordance with physical principles. In the context of building thermal dynamics, for example, past and current cooling HVAC inputs lead to impact zone temperature in future time steps:

$$\frac{\partial T_k^m}{\partial u_j^m} < 0, \forall 0 \le j < k \tag{6}$$

Similarly, the physical consistency with respect to the outside temperature in tropical regions (cooling case) can be defined as:

$$\frac{\partial T_k^m}{\partial T_j^{OA}} > 0, \forall 0 \le j < k \tag{7}$$

Lastly, the physical consistency with respect to the thermal topology between different rooms can be written as:

$$\frac{\partial T_k^{m_1}}{\partial T_j^{m_2}} > 0, \forall 0 \le j < k; m_1 \ne m_2; m_1, m_2 \in M \tag{8}$$

Where M represents the set of thermal zones in the building. Equation (8) shows that a temperature rise in zone m_1 leads to a higher temperature in an adjacent zone m_2 in future timesteps.

To satisfy the physically consistent criteria in Equation (6)-(8), the parameters in S-PCNN model Equation (4) hold the following:

$$a_m, b_m, c_m > 0, 1 - b_m - \sum_{m_{\text{adj}}} c_{m,m_{\text{adj}}} > 0; m, m_{\text{adj}} \in M \tag{9}$$

Where m_{adj} is all the zones that are adjacent to zone m. The proof of the proposition in Equation (9) is in [38]. The consistency of physics is enforced during the training process.

3.2.2. State-space representation

We define the room temperature of $m = 6$ thermal zones as the state vector:

$$\boldsymbol{T}_k = \begin{bmatrix} T_k^1 & T_k^2 & \cdots & T_k^6 \end{bmatrix}^\top \tag{10}$$

Since the HVAC input is designated for each VAV, the control vector has the identical dimension of the thermal zones $m = 6$:

$$\boldsymbol{u}_k = \begin{bmatrix} u_k^1 & u_k^2 & \cdots & u_k^6 \end{bmatrix}^\top \tag{11}$$

We can learn from the layout of the testbed that each room is exterior and the topology of adjacencies. We can write the state space form that follows Equation (4):

$$\boldsymbol{T}_{k+1} = \boldsymbol{A}\boldsymbol{T}_k + \boldsymbol{B}\boldsymbol{u}_k + \boldsymbol{C}T_k^{OA} + f_{\boldsymbol{NN}}(\boldsymbol{x}_k) \tag{12}$$

where

$$\boldsymbol{A} = \begin{pmatrix} p_1 & c_{12} & c_{13} & 0 & 0 & 0 \\ c_{12} & p_2 & c_{23} & c_{24} & c_{24} & c_{26} \\ c_{13} & c_{23} & p_3 & 0 & 0 & 0 \\ 0 & c_{24} & 0 & p_4 & 0 & 0 \\ 0 & c_{25} & 0 & 0 & p_5 & c_{56} \\ 0 & c_{26} & 0 & 0 & c_{56} & p_6 \end{pmatrix}, \boldsymbol{B} = \begin{pmatrix} a_1 & 0 & \cdots & 0 \\ 0 & a_2 & \cdots & 0 \\ \vdots & \vdots & \ddots & \vdots \\ 0 & 0 & \cdots & a_6 \end{pmatrix}$$

$$\boldsymbol{C} = \begin{bmatrix} b_1 & b_2 & \cdots & b_6 \end{bmatrix}^\top$$

where $p_1 = 1 - b_1 - \sum_{2,3} c_{1i}$, $p_2 = 1 - b_2 - \sum_{1,3,4,5,6} c_{2i}$, $p_3 = 1 - b_3 - \sum_{1,2} c_{3i}$, $p_4 = 1 - b_4 - \sum_{2,6} c_{4i}$, $p_5 = 1 - b_5 - \sum_{2,6} c_{5i}$, and $p_6 = 1 - b_6 - \sum_{2,5} c_{6i}$. $f_{\boldsymbol{NN}}(\boldsymbol{x}_k)$ is the neural network, a shared nonlinear function $\mathbb{R}^m \to \mathbb{R}^m$. The inputs $\boldsymbol{x}_k \in \mathbb{R}^m$ include the solar irradiation, in-room carbon dioxide concentrations, and MELs load, which impacts the room temperature regulations but are traditionally difficult to characterize in reduced-order models. It should be noted that $f_{\boldsymbol{NN}}(\boldsymbol{x}_k)$ and its input are independent of control variables. It allows us to compute $f_{\boldsymbol{NN}}(\boldsymbol{x}_k)$ separately over the prediction horizon and use it as an exogenous disturbance in the MPC setting.

Proposition 3.2. *(Stability of PCNN-MPC discrete-time system) The S-PCNN state-space model is asymptotically stable. For any bounded initial condition and zero exogenous input (including controls and the NN module), the states converge to zero, i.e.,* $||\boldsymbol{T}_0|| < \epsilon, \boldsymbol{u}_k = 0, \& \ f_{\boldsymbol{NN}}(\boldsymbol{x}_k) \Rightarrow \lim_{k\to\infty} ||\boldsymbol{T}_k|| = 0$.

The proof of Proposition 3.2 can be found in Appendix A.

3.2.3. MPC formulation: baseline and flexible cases

We used an MPC framework to control the system described in Equation (12). Therefore, at each time step k, a sequence of predicted control HVAC cooling input is computed by minimizing an objective function over the prediction horizon N. Only the control at instant k is subsequently deployed to the system.

The problem is defined as follows:

$$\text{minimize}_{\boldsymbol{u}} \quad \frac{1}{2}(\boldsymbol{T}_k - \boldsymbol{T}^{ref})^T \boldsymbol{Q}(\boldsymbol{T}_k - \boldsymbol{T}^{ref}) + \frac{1}{2}(\boldsymbol{u}_k - \boldsymbol{u}^{ref})^T \boldsymbol{R}(\boldsymbol{u}_k - \boldsymbol{u}^{ref}) \tag{13}$$

$$\text{subject to} \quad \boldsymbol{T}_{k+1} = \boldsymbol{A}\boldsymbol{T}_k + \boldsymbol{B}\boldsymbol{u}_k + \boldsymbol{C}T_k^{OA} + f_{\boldsymbol{NN}}(\boldsymbol{x}_k) \tag{14}$$

$$\boldsymbol{T}_{\min} \le \boldsymbol{T}_k \le \boldsymbol{T}_{\max} \tag{15}$$

$$\boldsymbol{u}_{\min} \le \boldsymbol{u}_k \le \boldsymbol{u}_{\max} \tag{16}$$

$$u_k^{\text{ref}} = \hat{a}_1 G_k^2 + \hat{a}_2 G_k T_k^{OA} + \hat{a}_3 G_k \tag{17}$$

Equation (13) minimizes the difference between the PV generation P_{PV} and the summation of the building demand P_{load}. Where $\boldsymbol{Q} \in \mathbb{R}^{6\times6}$ and $\boldsymbol{R} \in \mathbb{R}^{6\times1}$ are the weighting coefficient matrices for the room temperatures (states) and HVAC power inputs (controls), respectively. The $\boldsymbol{Q}$ weighting coefficient matrix serves as a penalty term for thermal comfort consideration, similar to [20].

For the constraints, Equation (14) is the dynamic equation built by the S-PCNN model. Equation (15) is the room temperature constraint varying between 25 °C and 28 °C, as they are the lower bound and upper bound of the thermostat adjustments in the building, respectively. Equation (16) is the torque limitation of the control, which is subjected to the FCU damper and valve positions. Equation (17) represents the dynamics of PV generation (as a function of solar irradiance and outdoor air temperature), which serves as the reference power input in this formulation. The derivation details of Equation (17) are illustrated in Appendix B.

To solve this optimal control problem, we designed a quadratic programming (QP) based MPC controller. The implementation details are shown in Appendix C. In the virtual implementations, two different setups of the MPC strategy were applied. The first one is the baseline MPC control (*MPC (flat-rate)*) where the control weighting coefficient matrix $\boldsymbol{R}$ remains constant throughout the simulation horizon, namely scaled by the quarterly regulated flat-rate tariff by EMA. On the other hand, we also present flexible MPC control (*MPC (RTP)*), where $\boldsymbol{R}$ is time-variant ($\boldsymbol{R}(k)$). The control penalty term $\boldsymbol{R}(k)$ is scaled by the real-time pricing (half-hourly WEP) at each time step.

3.2.4. MPC formulation: BESS

The primary state variable for the BESS is SoC_k, representing the state of charge at discrete time k. Given this, the evolution of the battery's state of charge over time is described by the difference equation:

$$SoC_{k+1} = SoC_k + \eta_k u_k^{BES} \Delta t \tag{18}$$

Where η_k is the discharging/charging efficiency of the BESS at timestep k, u_k^{BES} stands for the power either supplied to or drawn from the BESS at time k, and Δt represents the fixed time interval between two consecutive time steps. When $u_k^{BES} > 0$, the BESS is charging whereas when $u_k^{BES} < 0$, the BESS is discharging. Also, the discharging and charging processes of the BESS cannot be done simultaneously. The assumption underpinning this model is that the charging/discharging rate with the BESS remains invariant within each time interval Δt. This simplification is particularly useful for scenarios where a higher resolution modeling of rapid power fluctuations is unnecessary or where control actions are adjusted at a discrete regular interval.

We define the extended states including the room temperature of $m = 6$ thermal zones and BESS SoC_k:

$$\boldsymbol{Z}_k = \begin{bmatrix} T_k^1 & T_k^2 & \cdots & T_k^6 & SoC_k \end{bmatrix}^\top \tag{19}$$

The control variable vector also includes the discharging/charging power input to the BESS:

$$\boldsymbol{u}_k = \begin{bmatrix} u_k^1 & u_k^2 & \cdots & u_k^6 & u_k^{\text{BES}} \end{bmatrix}^\top \tag{20}$$

$$\text{minimize}_{\boldsymbol{u}} \quad \frac{1}{2}(\boldsymbol{Z}_k - \boldsymbol{Z}^{ref})^T \boldsymbol{Q}(\boldsymbol{Z}_k - \boldsymbol{Z}^{ref}) + \frac{1}{2}R(\sum_i^n u_k^i + u_k^{\text{BES}} - u^{ref})^2 \tag{21}$$

$$\text{subject to} \quad \boldsymbol{T}_{k+1} = \boldsymbol{A}\boldsymbol{T}_k + \boldsymbol{B}\boldsymbol{u}_k + \boldsymbol{C}T_k^{OA} + f_{\boldsymbol{NN}}(\boldsymbol{x}_k) \tag{22}$$

$$\boldsymbol{T}_{\min} \le \boldsymbol{T}_k \le \boldsymbol{T}_{\max} \tag{23}$$

$$\boldsymbol{u}_{\min} \le \boldsymbol{u}_k \le \boldsymbol{u}_{\max} \tag{24}$$

$$u_k^{\text{ref}} = \hat{a}_1 G_k^2 + \hat{a}_2 G_k T_k^{OA} + \hat{a}_3 G_k \tag{25}$$

$$SoC_{k+1} = SoC_k + \eta_k u_k^{BES} \Delta t \tag{26}$$

$$SoC_{\min} \le SoC_k \le SoC_{\max} \tag{27}$$

Where $SoC_{\min}$ is the minimum capacity of the BESS, set to be 25% of its nominal capacity, and $SoC_{\max}$ is the maximum capacity of the BESS, set to be 90% of its nominal capacity. In addition, the magnitude of discharging/charging power input $|u_k^{\text{BES}}|$ is also constrained by the maximum discharging/charging rate of the BESS. Lastly, the discharging/charging efficiency of the BESS η_k is subject to many factors, such as the discharging/charging rate, depth of discharge (DoD), battery temperature, and ambient temperature [48]. For simplicity, the discharging/charging efficiency η_k is assumed to be constant in this study.

It should be noted that now the objective function in Equation (21) minimizes the difference between the PV generation u^{ref} and the summation of the building load $\sum_i^n u_k^i$ and the battery discharging/charging power u_k^{BES} and the state factor η_k. When $u_k^{\text{BES}} > 0$, the BESS is charging, and the PV generation is surplus, i.e., at least sufficient to supply the building load demand. When $u_k^{\text{BES}} < 0$, the battery is discharging, which means the building load is supplied by the battery and the PV collectively.

4. Numerical results

In this section, we present the numerical results. The building thermal dynamic modeling results using the adopted S-PCNN model as illustrated in Section 3.2.1 are analyzed in Section 4.1. Secondly, the control results of the proposed MPC framework (Section 3.2.3) under two different pricing regimes are presented in Section 4.2. Finally, the control results comparison between the proposed MPC framework with (Section 3.2.4) and without BESS incorporation is exhibited in Section 4.3.

4.1. S-PCNN modeling results

This section provides a detailed analysis of the prediction performance of the adopted S-PCNN model. The S-PCNN model is trained to be capable of predicting the temperature of the multi-zones over a sequence of one day (24 hours), with an interval of 5 minutes (288 data points). The training period spanned from February to April 2022, while the test data was sourced from May 2022. To evaluate the S-PCNN model performance in terms of its extrapolation ability and prediction consistency, we trained and validated the model with 20 random seeds and computed the propagation of mean absolute error (MAE) over the validation sequences. Fig. 3 shows each model's mean and standard deviation of MAE from a one-step prediction horizon to 288 steps. Except for Room 4, the mean values of MAE of other zones are less than 0.35 °C. It is noted that both the mean and standard deviation MAE generally attain stability when the prediction horizon reaches 10 hours. Also, the standard deviation of MAEs from different random seeds is less than 0.05 °C for all six zones. These results underscore that the S-PCNN model achieves state-of-the-art accuracy and demonstrates consistency in training outcomes.

The S-PCNN modeling performance is also analyzed with a group of metrics well-known for evaluating the accuracy of prediction, namely mean absolute error (MAE), root-mean-square error (RMSE), and mean

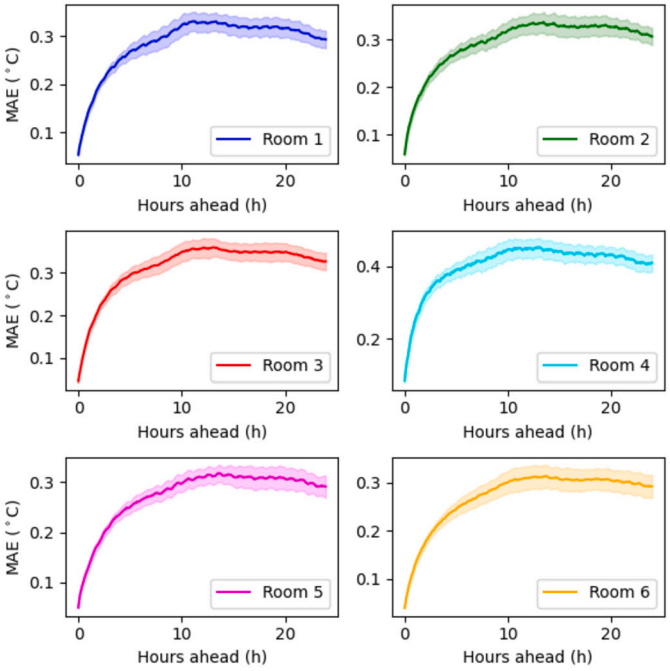

Fig. 3. Mean and standard deviation of the MAE at each time step of the prediction horizon for the S-PCNN of six rooms in the testbed, where the statistics were computed from 20 random seeds.

Table 2
The results indicate that the adopted S-PCNN model exhibits stability over a one-day-long extrapolation. It outperforms the RC network model for different prediction horizons.

Prediction Horizon	MAE		RMSE		MAPE	
	S-PCNN	RC	S-PCNN	RC	S-PCNN	RC
1 Hour	**0.1422**	0.3033	**0.1951**	0.364	**0.52%**	1.11%
3 Hour	**0.2223**	0.4618	**0.2939**	0.5643	**0.82%**	1.69%
6 Hour	**0.2726**	0.607	**0.3501**	0.7523	**1.00%**	2.23%
12 Hour	**0.3176**	0.799	**0.4051**	0.9641	**1.17%**	2.94%
24 Hour	**0.3033**	0.5511	**0.3893**	0.7084	**1.23%**	2.02%

absolute percentage error (MAPE). To benchmark the prediction performance of the adopted S-PCNN model, we compare it with a resistor-capacitor (RC) network model, a commonly used data-driven model in building temperature modeling. The details of the RC network model are delineated in Appendix D. More information can be found in previous work [20].

Table 2 reports the MAE, RMSE, and MAPE of the adopted S-PCNN and the RC network model. It can be observed that the adopted S-PCNN outperforms the RC network over short, medium, and long prediction horizons. The largest MAE or the adopted S-PCNN is 0.3176, RMSE is 0.4051, and the largest MAPE is 1.23%. All three metrics remain low throughout the entire one-day prediction horizon. The results show that the S-PCNN maintains a high degree of accuracy and stability, even over the course of a full day's prediction horizon. This consistent performance highlights the S-PCNN's robustness and reliability for long-term extrapolation in building temperature prediction.

In addition, we tested the model's prediction ability of "free-floating" thermodynamics of the testbed, i.e., there is no HVAC power input during the reduction horizon. Under free-floating mode, it can reveal if the model captures the inherent thermodynamics and heat transfer processes between building envelopes, outdoor conditions, and internal disturbances. To observe free-floating temperatures of the multi-zone testbed and assess the prediction results of the S-PCNN model under these circumstances, we picked up a weekend in May 2022 to compare the ground-truth room temperatures and the extrapolation

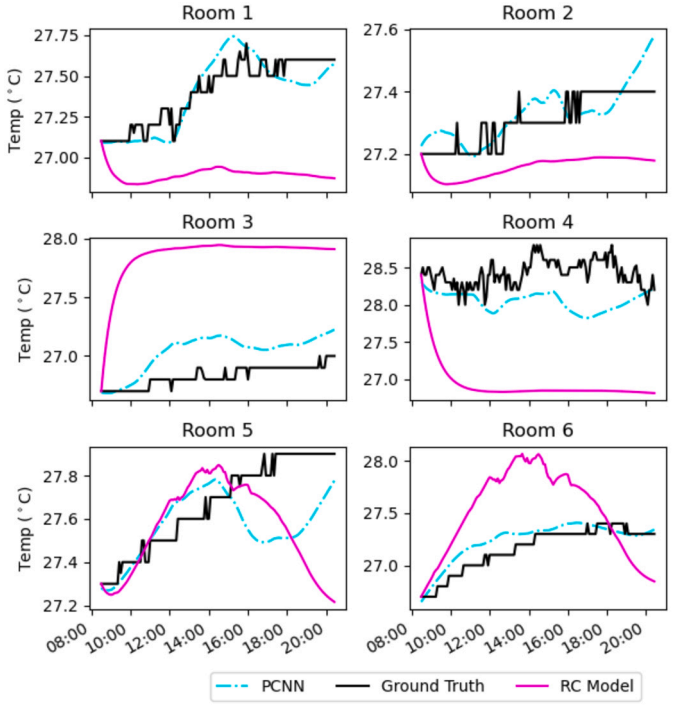

Fig. 4. Temperature predictions of the RC model and the S-PCNN model and their comparisons to the ground truth temperature profiles when the HVAC control input is zero, i.e., the building is in free-floating mode.

prediction of the S-PCNN model over a 12-hour prediction horizon. We also include the RC network model for comparison, as detailed in [20], were also presented for comparison, as depicted in Fig. 4. Based on the figure, it is evident that the S-PCNN model exhibits a substantially lower tracking error in comparison to the RC network model when the HVAC input is turned off. Furthermore, the extrapolated predictions generated by the S-PCNN model closely adhere to the ground truth temperature. These outcomes indicate that the S-PCNN model can effectively capture the inherent thermodynamic characteristics and forecast the free-floating behavior by retaining the physical consistency. It is worth noting that this comparison might not be entirely equitable due to discrepancies in the training mechanisms and data availability between the two models. Further investigations are required to provide a more thorough comparison between these two distinct data-driven modeling methods.

4.2. Baseline and flexible MPC results

This section presents the numerical simulation results of two MPC operations and compares them with the baseline control. The MPC strategies, *MPC (flat-rate)* and *MPC (RTP)* were implemented as two prospective flexible operations. The baseline control utilized the ground-truth BAS data for the HVAC control inputs, and the room temperatures were emulated using the S-PCNN model instead of the ground-truth data. The room temperature set point in the baseline control is 26.5 °C. Meanwhile, to improve thermal comfort, the room temperature set point under two MPC scenarios is set to 26 °C, as it achieves neutral thermal sensation under the default ceiling fan speed [20]. The thermal comfort weighting coefficient matrix $\boldsymbol{Q} = q\boldsymbol{I}$ weighting coefficient matrix is scaled by $q = 10$, whereas the control coefficient matrix $\boldsymbol{R}_k = price_k \boldsymbol{I}$. The thermal comfort weighting scalar q is determined based on heuristics, and can be adjusted to pursue higher thermal acceptability if needed. The electricity price factor $price_k$ in the context of *MPC (flat-rate)* operation determined using the regulated flat rate set by EMA for the second quarter of the year 2022, is equivalent to 0.2794 Singapore dollars per kWh. Conversely, in the *MPC (RTP)* scenario, the

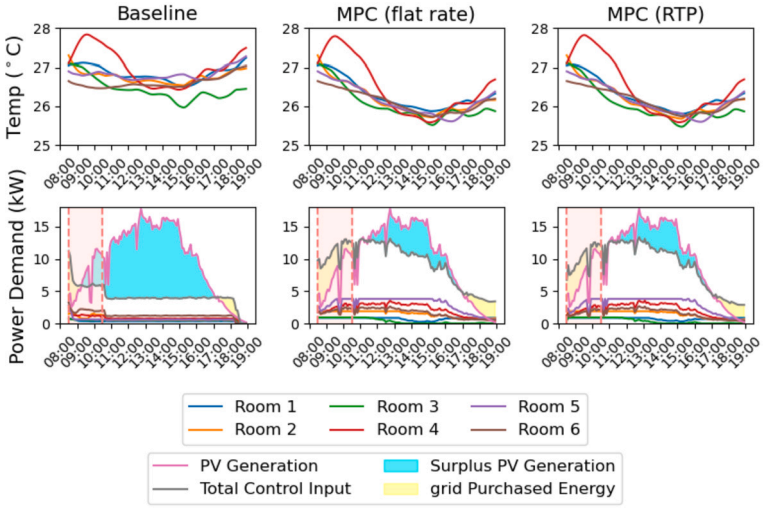

Fig. 5. The comparison of control behaviors of baseline control, the MPC control strategy with time-invariant flat-rate electricity pricing coefficient for penalizing controls, and the MPC control strategy with time-variant real-time electricity pricing coefficient for penalizing controls.

electricity price factor $price_k$ is based on historical data of WEP, which is subject to fluctuation every half-hour.

The numerical simulation was conducted for two weeks in May 2022 on the virtual testbed. The control strategies were conducted during the peak demand hours in Singapore, namely from 8 a.m. to 6 p.m. [49]. Fig. 5 shows the comparison between the typical control behaviors of three different operation strategies. It can be observed that for the baseline control, the constant room temperature set points achieved a stable energy consumption profile. Conversely, the energy consumption profile under *MPC (flat-rate)* circumstance followed the real-time on-site PV generation. The total load demand increased gradually in the morning to match the rise of the PV generation, and it subsequently winded down in the late afternoon. This approach took advantage of the building's thermal mass, allowing room temperatures to increase gradually. The *MPC (RTP)* strategy exhibited a load profile similar to that of *MPC (flat-rate)*. However, it should be noted that the load was more contracted PV generation during the early morning period (shaded in light pink). This can be attributed to the control penalty term in the *MPC (flat-rate)* setting, which varied throughout the day in response to the half-hourly WEP fluctuations. WEP typically has two peaks, around 9 a.m. and 4 p.m. The control inputs were subject to greater penalties during these timeframes, resulting in the framework's avoidance of excessive electricity purchases during these timeframes.

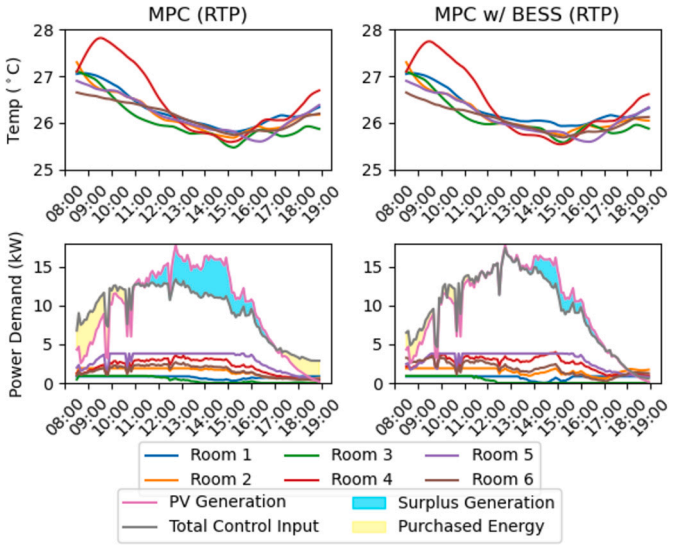

Fig. 6. The comparison of the MPC control strategy with time-invariant flat-rate electricity pricing coefficient for penalizing controls and the same MPC control strategy with BESS added.

4.3. BESS-added MPC results

To investigate the impact of battery energy storage systems (BESS) on the improvement of building energy flexibility, a fully integrated battery system is added to the *MPC (RTP)* framework virtually. The system has a 13.5 kWh usable capacity and a 5 kW maximum discharging/charging rate. The BESS is sized based on the peak load of the virtual testbed. The nominal capacity, charging and discharging rates, and suggested SoC range of the BESS are determined based on a commercial model that is available in Singapore with the closest capacity to the average daily peak load of the testbed.

Fig. 6 shows that the summation of the building load and the battery discharging/charging power closely followed the PV generation when the BESS is added, compared to the *MPC (RTP)* framework without BESS. In the early morning and late afternoon periods, when the PV generation fell short of meeting the building's load requirements, the battery discharged power to fulfill the demand. As a result, the purchased energy during these periods is considerably reduced. Furthermore, around noon, when the PV generation was abundant, the battery stored surplus PV power for future utilization.

Fig. 7 depicts the discharging/charging power and the SoC patterns during the simulation horizon. It indicates that in the morning, the BESS was discharging at its maximum power rate, but the collective power supply from the BESS and the PV generation still could not fill up the building's load requirements, and purchased energy can be observed. In the afternoon, the BESS was fully charged after the peak abundance of the PV generation and reached its maximum SoC. Therefore, the excessive PV generation could not be absorbed by the BESS anymore. A battery system with a larger capacity and greater discharging/charging power rate allowance is needed to improve further the trajectory following between the PV generation and the combined sum of the building load and the battery discharging/charging power.

4.4. Energy flexibility evaluation

4.4.1. Demand decrease percentage and energy decrease percentage

The daily power demand and energy consumption profiles over the two-week experiment period (Nine school days are presented.) are shown in Fig. 8. The corresponding energy flexibility KPIs, demand decrease percentage decrease (PDS), and energy decrease percentage

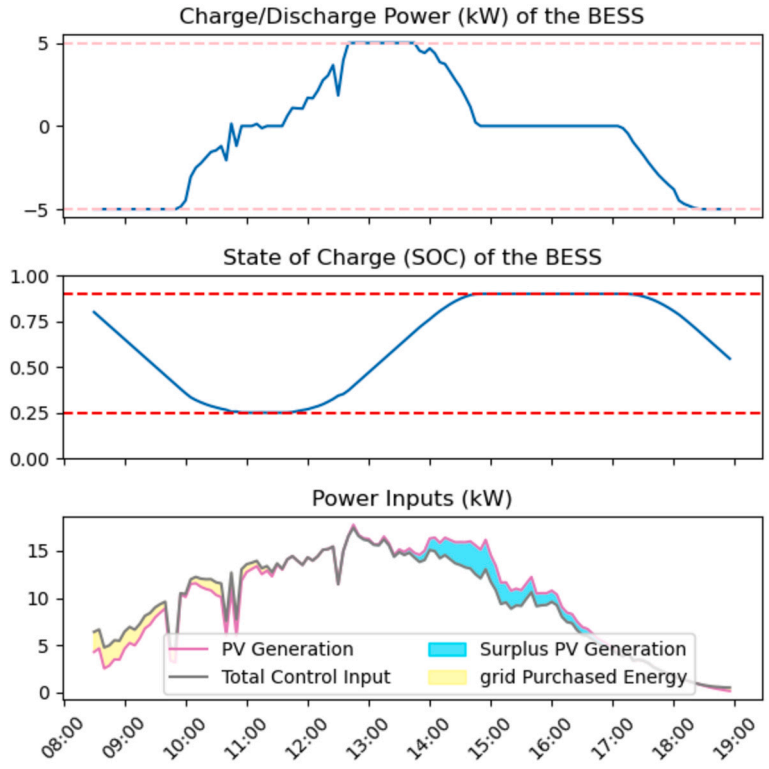

Fig. 7. The discharging/charging power, SoC, PV generation, and total HVAC control input aligned by timestamps. The pink dashed lines in the top figure show the maximum rated discharging/charging power of the specified BESS, and the red dashed lines in the middle figure show the upper and lower bounds of SoC.

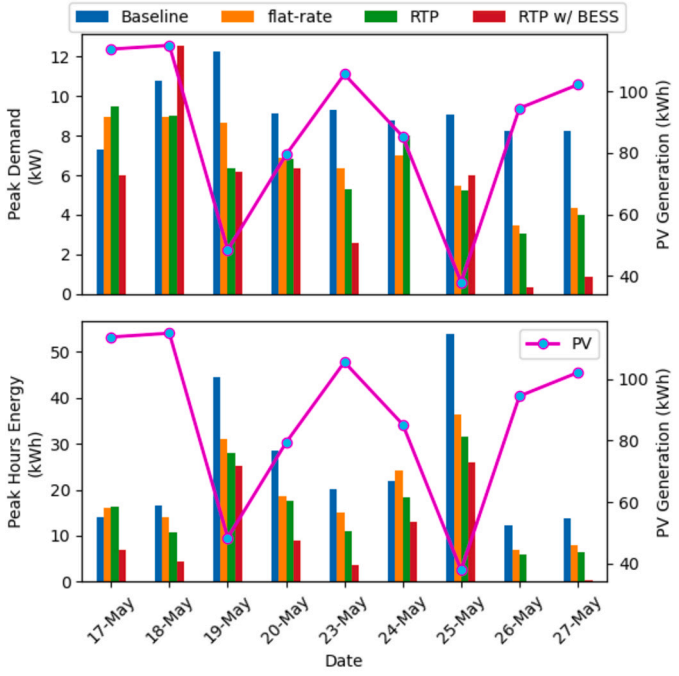

Fig. 8. Above: The daily peak demand comparison between the baseline operation, *MPC (flat-rate)*, *MPC (RTP)*, and *MPC + BESS (RTP)* scenarios. Below: The daily energy consumption comparison between the baseline operation, *MPC (flat-rate)*, *MPC (RTP)*, and *MPC + BESS (RTP)* scenarios.

(EDP) are shown in Table 3. It is noteworthy that the testbed exhibited a declining trend in energy consumption, following the order of the baseline controls *MPC (flat-rate)*, *MPC (RTP)*, and *MPC + BESS (RTP)* operation scenarios, Also, A negative correlation between the energy consumption during peak hours and daily on-site PV generation can be observed. This relationship signifies that as the on-site PV generation increases, the building load could be offset by the generation, so the purchased energy decreases. The results indicate that including the real-time pricing factor in the MPC control framework and adding a BESS to the building system can improve the energy efficiency of the building.

Table 3
PDS and EDS.

KPI	Date	MPC (flat-rate)	MPC (RTP)	MPC w/BESS (RTP)
PDS/EDS	May 17	-23%-/15%	-30%/-18%	17%/51%
	May 18	17%/15%	17%/35%	-16%/74%
	May 19	29%/30%	48%/37%	50%/43%
	May 20	25%/34%	25%/38%	30%/68%
	May 21	31%/25%	43%/46%	72%/82%
	May 24	20%/10%	9%/17%	100%/41%
	May 25	40%/32%	43%/41%	34%/52%
	May 26	58%/42%	63%/51%	96%/98%
	May 27	48%/43%	51%/54%	89%/97%
	Average	27%/22%	30%/34%	52%/67%

On the other hand, though a general trend of the peak power demand decline can be observed, the peak power varied among the different scenarios. The peak power demand is sensitive to the prediction of real-time on-site PV generation subject to Equation (17). For example, in cases where the prediction horizon overestimates PV generation, the controller may optimize for more aggressive control inputs. As a result, the actual PV generation may fall short of meeting the building's load requirements, necessitating an increased reliance on grid energy. However, it is noteworthy that the BESS can mitigate such situations, as shown in Table 3. The BESS can step in when the PV generation is insufficient to cover the load demand, thus reducing the amount of purchased energy, addressing the mismatch between predicted and actual PV generation, and ensuring a more stable energy supply.

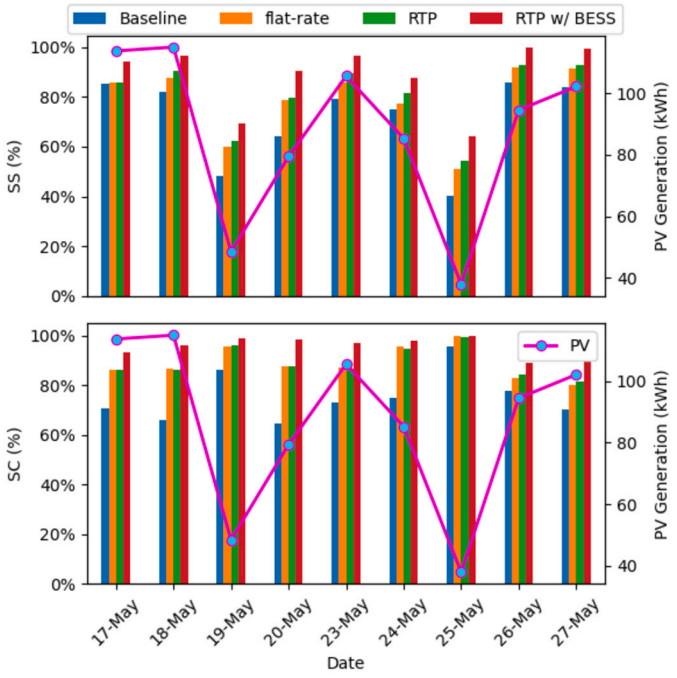

Fig. 9. Above: The daily average self-sufficiency rate comparison between the baseline operation, *MPC (flat-rate)*, *MPC (RTP)*, and *MPC + BESS (RTP)* scenarios. Below: The daily average self-consumption rate comparison between the baseline operation, *MPC (flat-rate)*, *MPC (RTP)*, and *MPC + BESS (RTP)* scenarios.

Table 4
SS and SC.

KPI	Date	MPC (flat-rate)	MPC (RTP)	MPC w/BESS (RTP)
SS/SC	May 17	1%/15%	0%/15%	9%/22%
	May 18	6%/21%	8%/20%	14%/30%
	May 19	12%/9%	14%/10%	21%/13%
	May 20	15%/23%	16%/23%	26%/34%
	May 23	7%/14%	10%/13%	17%/24%
	May 24	2%/21%	7%/20%	13%/23%
	May 25	11%/4%	14%/4%	24%/4%
	May 26	6%/5%	7%/6%	14%/11%
	May 27	7%/10%	9%/11%	16%/20%
	Average	7%/14%	10%/14%	17%/20%

4.4.2. Self-sufficiency and self-consumption

Self-sufficiency (SS) evaluates if the amount of the on-site generation is sufficient to fill the energy needs of the building. Greater SS rates indicate the abundance of on-site renewable energy generation. Self-consumption (SC) quantifies the amount of the on-site generation that is directly consumed by the building and the battery. Greater SS rates exhibit a higher utilization of renewable energy. The daily mean SS and SC rates over the two-week experiment period (Nine school days are presented.) are shown in Fig. 9. The comparisons of SS and SC are shown in Table 4. It is obvious that a more plentiful daily PV generation yielded higher SS and lower SC for all four scenarios. Both SS and SC increased progressively when more advanced control measures were used.

5. Discussion

5.1. Impact of pricing schemes to energy flexibility

One of the research objectives of this study is to investigate the impact of different electricity pricing schemes on the MPC framework. Two electricity pricing options in Singapore were considered: the regulated flat rate tariff and RTP based on WEP. The bottom subplots in Fig. 10 present the regulated flat rate tariff ($0.2794/kWh) for the second quarter of 2022 announced by EMA in red. The blue curves illustrate the fluctuations of the half-hourly WEP during peak demand hours for four consecutive days during the virtual experiment. WEP on May 19 and May 20 exhibits the typical pattern of the dynamic tariff, featuring two peaks, one in the morning and the other one in the afternoon. We can observe that WEP falls below the regulated flat rate after the afternoon peak, and the power demand under the *MPC (RTP)* scenario increases, surpassing that of *MPC (flat-rate)*. On May 18, the WEP is considerably higher than the regulated day for entire peak hours. Consequentially, the total control power associated with *MPC (RTP)* operation is subject to more substantial penalties compared to *MPC (flat-rate)*, as shown in the top subplot for May 18. During entire peak hours, the total control input becomes more closely aligned with PV generation.

The observations reflect the sensitivity of power demand as the control variables in the proposed MPC framework to WEP fluctuations and highlight how the pricing scheme can influence control decisions. Leveraging the dynamic nature of WEP can, in turn, contribute to improved energy efficiency and increased utilization of on-site renewable energy generation.

5.2. Impact of thermal comfort weighting matrix on MPC

Despite electricity pricing schemes, the degree to which thermal comfort compromises also influences the control strategies. It can be noted from the temperature and control comparison in Fig. 11 that the greater the thermal comfort penalty was, the larger the total control inputs it required and, subsequently, the faster the room temperature converged to the set point. In addition, after 14:00 pm, when the temperature reached the set point, the controller continued to lower the temperatures when the thermal comfort penalty was small ($q = 0.1, 1, 10$), resulting in greater utilization of the PV generation, but the energy consumption might not be necessary. Furthermore, we can also observe how the thermal comfort weighting coefficient impacted battery usage. The higher demand caused by the larger thermal comfort penalty led to a larger battery discharging power. Also, it was easier for the BESS to reach its minimum SoC when the power demand was high. For a larger thermal comfort weighting coefficient, we could possibly upsize the BESS to ensure the energy flexibility of the building while maintaining thermal comfort. The observations demonstrate that thermal comfort considerations are a crucial factor influencing control strategies alongside electricity pricing schemes. In the present study, the thermal comfort weighting scalar $q = 10$ selected is time-invariant. Future work will explore online optimization of a time-variant optimal thermal comfort weighting scalar considering the dynamic fluctuations in electricity prices (which impact the control penalty $\mathbf{R}$) and real-time thermal acceptability.

5.3. Petential of PCNN-MPC framework

In the present work, we developed an MPC framework based on the recently proposed PCNN model. This framework was empirically validated using real-world data from a tropical commercial building. The general formulation of the control problem, as delineated in Equation (12) and (13), exhibits applicability beyond the present case study, making it suitable for a variety of buildings facing challenges in energy flexibility. Control variables can be tailored to align with the distinct HVAC systems of the targeted buildings. Moreover, the inputs for the black-box component of the model can be customized based on the data availability in specific deployment scenarios. In instances where BAS and IEQ are partially or entirely unavailable, the framework can incorporate temporal features such as the time of day and the day of the week.

In the case study, the neural network module inputs are solar irradiation, in-room carbon dioxide concentrations, and MELs load. These

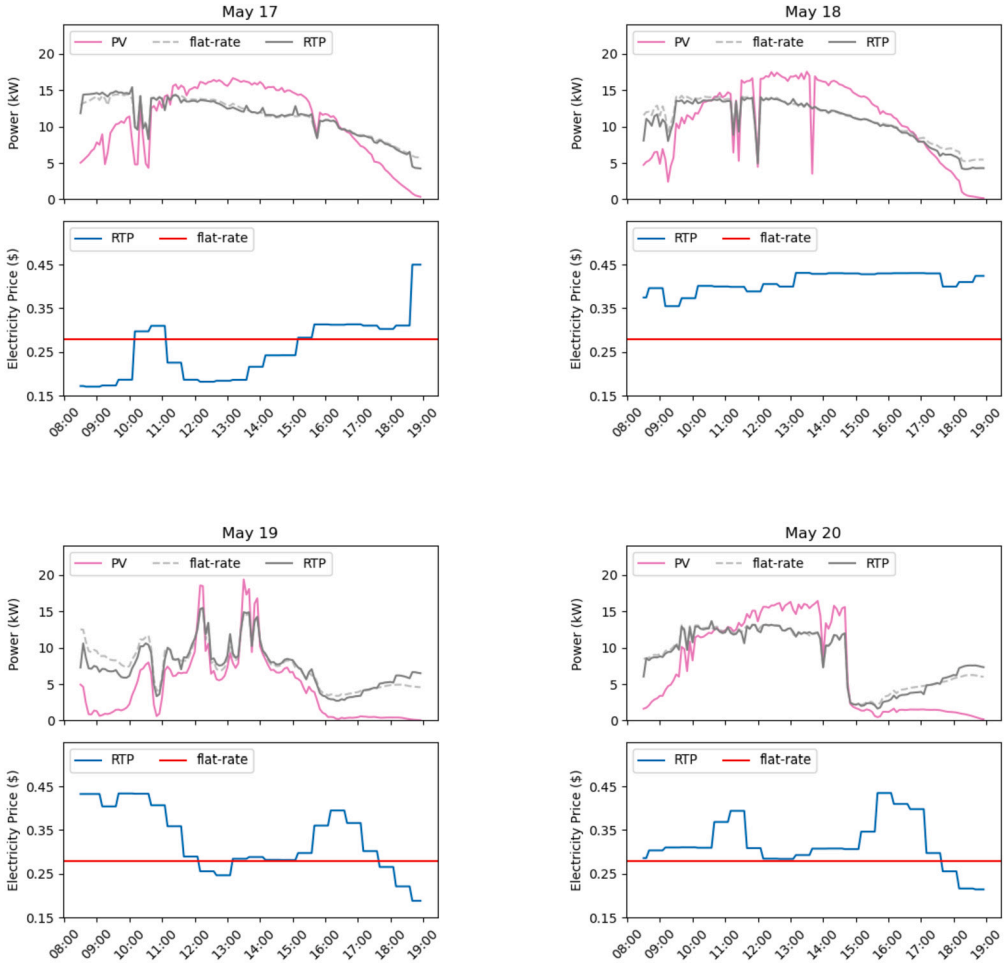

Fig. 10. The top subplot of each day shows the PV generation and the total control input under *MPC (flat-rate)* and *MPC (RTP)* operations. The bottom subplot of each day shows the corresponding regulated flat rate and RTPs.

inputs collectively encapsulate the effects of solar heat gain, occupancy load, and heat dissipation from MELs on room temperature variations. Such impacts are challenging to quantify precisely in reduced-order models. Furthermore, the black-box module and its inputs are independent of the physics-consistent module and control variables. It allows the framework to use the neural network as an exogenous input over the prediction horizon.

5.4. Limitations and future work

Several limitations are involved with the MPC framework, and the case study presented. Firstly, the proposed MPC framework requires intensive data. Data from several dimensions, including BAS, IEQ, and weather data, are involved in constructing the model and implementing the control strategy. Several data, such as occupancy, lighting, and MELs, are considered difficult to acquire in the data-driven EF quantification framework, as illustrated in Fig. 1 and Fig. 2. Developing and applying the proposed PCNN-MPC framework might be challenging in practice.

Secondly, the modeling and operation of the BESS are simplified in this case study. In reality, the charging/discharging power of the battery can be affected by several factors, such as SoC, outdoor air temperature, and the life-cycle cost that needs to be calculated during each charging/discharging circle. In addition, the return on investment (ROI) of the BESS is not discussed.

There are opportunities for future research and applications to improve building energy flexibility with the proposed framework:

- **Compare the effectiveness of the proposed MPC framework with different data-driven models**: In Fig. 4, we briefly compared the prediction results of the S-PCNN model and an R2C1 model on the same testbed. However, as we mentioned before, it may not be a fair comparison, as the two models' training mechanisms and data availabilities are not completely aligned. To comprehensively investigate the impact of different data-driven models, a rigorously aligned training and validation process is required, and notable conventional data-driven methods such as autoregressive–moving-average models and artificial neural networks (ANN) based models need to be evaluated in addition to RC models.
- **Control-oriented Modification of S-PCNN structure**: In the case study, the HVAC input is implied as a power input and calculated from BAS data. However, in real-world conditions, the HVAC power input is a dependent variable yielding several distinct control variables, such as VAV damper positions and chilled water supply temperature. The structure of the S-PCNN model needs to be modified in order to implement the real-world control variables into the model directly.

6. Conclusion

In this paper, we presented a case study that evaluates the influence of different electricity pricing mechanisms and the impact of a local battery energy storage system (BESS) on building energy flexibility controls and operations. The case study considers a net-zero energy office building in a tropical region with on-site solar photovoltaic (PV) available.

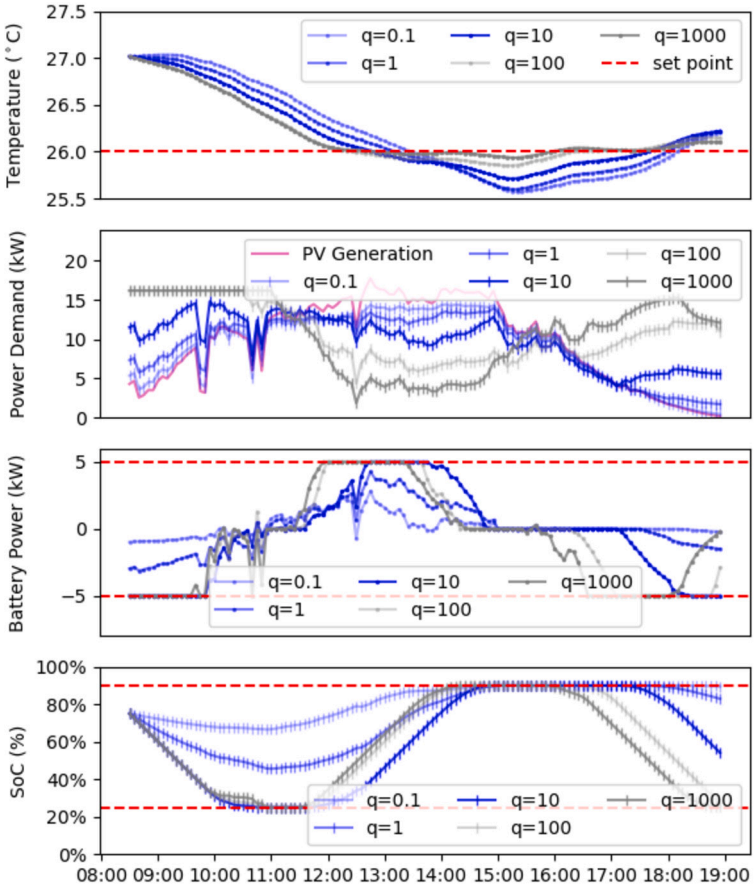

Fig. 11. From top to bottom: the average room temperature, power demand, the discharging/charging power, and SoC of different state (temperature) weighting coefficient matrices in *MPC+BESS (RTP)* operation during a day.

We proposed a model predictive (MPC) framework incorporating the Physically Consistent Neural Network (PCNN) model for quantifying building energy flexibility and demonstrated the framework using real-world data. Three flexible operations were discussed: MPC with the regulated flat-rate configuration, MPC with real-time pricing configuration, and MPC with real-time pricing configuration when an on-site BESS is available. Based on the numerical simulation results, the proposed MPC framework with flat-rate configuration achieved 27% demand decrease and 22% energy decrease compared to the baseline control, whereas the real-time pricing configuration achieved 30% demand decrease and 34% energy decrease. Also, the proposed MPC framework with BESS improved the building self-sufficiency and the PV self-consumption by 17% and 20% from the baseline, respectively. The results show that PV and BESS can improve energy efficiency, address model mismatch in the MPC framework, and ensure a more stable energy supply for tropical buildings. Moreover, the observations indicate that dynamic pricing could be beneficial to leverage building energy flexibility for control decisions.

Additionally, we designed a novel PCNN-MPC framework with intensive mathematical details and formally proved its stability as a discrete-time system. Future research can leverage the proposed framework for data-driven energy flexibility quantification with different buildings, data availabilities, objectives, and KPIs.

CRediT authorship contribution statement

Wei Liang: Writing – review & editing, Writing – original draft, Software, Methodology, Investigation, Formal analysis, Data curation, Conceptualization. **Han Li:** Writing – review & editing, Methodology. **Sicheng Zhan:** Writing – review & editing, Methodology, Data curation. **Adrian Chong:** Writing – review & editing, Writing – original draft, Resources, Methodology, Conceptualization. **Tianzhen Hong:** Writing – review & editing, Supervision, Project administration, Methodology, Funding acquisition, Conceptualization.

Declaration of competing interest

The authors declare that they have no known competing financial interests or personal relationships that could have appeared to influence the work reported in this paper.

Data availability

Data will be made available on request.

Acknowledgements

The LBNL team's work was supported by the Assistant Secretary for Energy Efficiency and Renewable Energy, Office of Building Technologies of the United States Department of Energy, under Contract No.DEAC02-05CH11231.

Appendix A. Proof for stability of S-PCNN discrete-time system

For a generalized S-PCNN system in Equation (12), the initial response is:

$$\begin{aligned}\boldsymbol{T}_{k+1} &= \boldsymbol{A}\boldsymbol{T}_k + \boldsymbol{B}\boldsymbol{u}_k + \boldsymbol{C}\boldsymbol{T}_k^{OA} + f_{\boldsymbol{NN}}(\boldsymbol{x}_k)\\ &= \boldsymbol{A}(\boldsymbol{A}\boldsymbol{T}_{k-1} + \boldsymbol{B}\boldsymbol{u}_{k-1} + \boldsymbol{C}\boldsymbol{T}_{k-1}^{OA} + f_{\boldsymbol{NN}}(\boldsymbol{x}_{k-1}))\\ &\quad + \boldsymbol{B}\boldsymbol{u}_k + \boldsymbol{C}\boldsymbol{T}_k^{OA} + f_{\boldsymbol{NN}}(\boldsymbol{x}_k)\\ &= \boldsymbol{A}^{k+1}\boldsymbol{T}_0 + \sum_{i=0}^{k}\boldsymbol{A}^{k-i}\boldsymbol{B}\boldsymbol{u}_i + \sum_{i=0}^{k}\boldsymbol{A}^{k-i}\boldsymbol{C}\boldsymbol{T}_i^{OA} + \sum_{i=0}^{k} f_{\boldsymbol{NN}}(\boldsymbol{x}_i)\end{aligned} \tag{A.1}$$

The stability condition of a discrete-time system described in Equation (A.1) is that $\lim_{k\to\infty}\boldsymbol{A}^k = 0, \forall ||\boldsymbol{T}_0|| < \epsilon$. Therefore, the eigenvalues of $\boldsymbol{A}$ must be inside unit circle, i.e., $|\lambda_{\boldsymbol{A}}| < 1$.

The generalized form of $\boldsymbol{A}$ in S-PCNN model can be written as:

$$A_{ii} = 1 - b_i - \sum_{i\neq j}^{m} c_{ij} \tag{A.2}$$

$$A_{ij} = A_{ji} = c_{ij} \tag{A.3}$$

It is worth remarking that $\boldsymbol{A}$ is a symmetric matrix. As a result, the eigenvalues $\lambda_{\boldsymbol{A}}$ are real. According to Geršhgorin's Theorem, every eigenvalue of matrix $\lambda_{\boldsymbol{A}}$ satisfies:

$$|\lambda - A_{ii}| \leq \sum_{j\neq i}^{m} |A_{ij}| \tag{A.4}$$

Remember Remark 3.1 that $b_i, c_{ij} > 0$ and $1 - b_i - \sum_{i\neq j}^{m} c_{ij} > 0$ Based on Equation (A.2) and Equation (A.2), Geršhgorin's Theorem in Equation (A.4) can be rewritten as

$$\begin{aligned}&|\lambda - A_{ii}| \leq \sum_{j\neq i}^{m} |A_{ij}|\\ \Rightarrow &|\lambda - (1 - b_i - \sum_{i\neq j}^{m} c_{ij})| \leq \sum_{j\neq i}^{m} |c_{ij}| = \sum_{j\neq i}^{m} c_{ij}\\ \Rightarrow &-\sum_{j\neq i}^{m} c_{ij} < \lambda - (1 - b_i - \sum_{i\neq j}^{m} c_{ij}) < \sum_{j\neq i}^{m} c_{ij}\\ \Rightarrow &1 - b_i - 2\sum_{i\neq j}^{m} c_{ij} < \lambda < 1 - b_i\\ \Rightarrow &2(1 - b_i - \sum_{i\neq j}^{m} c_{ij}) - (1 - b_i) < \lambda < 1 - b_i\end{aligned}$$

From Remark 3.1, it is easily to observe that $-1 < 0 - (1 - b_i) < 2(1 - b_i - \sum_{i\neq j}^{m} c_{ij}) - (1 - b_i)$ and $1 - b_i < 1$. As a result, the eigenvalues of $\boldsymbol{A}$ satisfy that $-(1 - b_i) < \lambda_{\boldsymbol{A}} < 1 - b_i$, i.e., for every eigenvalue of $\boldsymbol{A}$, we have

$$|\lambda_{\boldsymbol{A}}| < 1 - b_i \tag{A.5}$$

Since the physics consistency ensures that $b_i > 0$, it is obvious that $|\lambda_{\boldsymbol{A}}| < 1$. We can conclude that the discrete-time dynamic system without controls and disturbances is asymptotic stable.

Appendix B. PV modeling details

The maximum power output of rooftop PV panels depends on varying solar irradiance and cell temperature. A validated equation based on Osterwald's method that considers both the theoretical accuracy and computational simplicity is as follows [50]:

$$P(k) = P_{\text{STC}}^{*}\frac{G(k)}{G_{\text{STC}}}(1 + \frac{\alpha_p}{100}(T_c(k) - T_{c,\text{STC}})) \tag{B.1}$$

In Equation (B.1), the cell temperature $T(c)$ is a time-variant parameter and can be estimated as:

$$T_c(k) = T_{oa}(k) + (NOCT - T_{oa,\text{ref}})\frac{G(k)}{G_{\text{ref}}} \tag{B.2}$$

Combining Equations (B.1) and (B.2), we obtain the real-time maximum power output of rooftop PV array dependent on the external weather disturbances, global horizontal irradiance $G(k)$ and outdoor air dry-bulb temperature $T_{oa}(k)$:

$$\begin{aligned}P(k) &= P_{\text{STC}}^{*}\frac{G(k)}{G_{\text{STC}}}(1 + \frac{\alpha_p}{100}(T_{oa}(k) + (NOCT - T_{oa,\text{ref}})\frac{G(k)}{G_{\text{ref}}} - T_{c,\text{STC}}))\\ &= \frac{\alpha_p}{100}\frac{P_{\text{STC}}^{*}(NOCT - T_{oa,\text{ref}})}{G_{\text{STC}}G_{\text{ref}}}G^2(k) + \frac{\alpha_p}{100}\frac{P_{\text{STC}}^{*}}{G_{\text{STC}}}G(k)T_{oa}(k)\\ &\quad + (1 - \frac{\alpha_p}{100}T_{c,\text{STC}})\frac{P_{\text{STC}}^{*}}{G_{\text{STC}}}G(k)\\ &= a_1G^2(k) + a_2G(k)T_{oa}(k) + a_3G(k)\end{aligned} \tag{B.3}$$

where

$$a_1 = \frac{\alpha_p}{100}\frac{P_{\text{STC}}^{*}(NOCT - T_{oa,\text{ref}})}{G_{\text{STC}}G_{\text{ref}}}$$

$$a_2 = \frac{\alpha_p}{100}\frac{P_{\text{STC}}^{*}}{G_{\text{STC}}}$$

$$a_3 = (1 - \frac{\alpha_p}{100}T_{c,\text{STC}})\frac{P_{\text{STC}}^{*}}{G_{\text{STC}}}$$

Note that a_1, a_2, and a_3 all consist of manufacturer-prescribed coefficients tested under standard operating conditions (SOC) and/or Standard Test Conditions (STC), which can be considered as constant in this case. Based on Equation (B.3), the PV forecast can be obtained via multiple linear regression (MLR):

$$\hat{P}(k) = \hat{a_1}G^2(k) + \hat{a_2}G(k)T_{oa}(k) + \hat{a_3}G(k) + \varepsilon \tag{B.4}$$

Appendix C. Quadratic programming based MPC controller

To solve this optimal control problem, we can design a quadratic programming (QP) based MPC controller by re-construct the problem as follows:

$$\text{minimize}_z \quad \frac{1}{2}z^T Pz + q^T z \tag{C.1}$$

$$\text{subject to} \quad D_{eq}z = d_{eq} \tag{C.2}$$

$$C_{ineq}z \leq d_{ineq} \tag{C.3}$$

where the equality constraint $D_{eq}z = d_{eq}$ can be explicitly expressed as:

$$\begin{bmatrix} B & -I & & & & \\ & A & B & -I & & \\ & & & \ddots & & \\ & & & & A & B - I \end{bmatrix}\begin{bmatrix} u_1 \\ T_2 \\ u_2 \\ \vdots \\ T_{N-1} \\ u_{N-1} \\ T_N \end{bmatrix} = \begin{bmatrix} -AT_1 - CT_1^{OA} - NN(x_1) \\ -CT_2^{OA} - NN(x_2) \\ \vdots \\ -CT_{N-1}^{OA} - NN(x_{N-1}) \end{bmatrix}$$

$N = 12$ (one hour) is the prediction horizon. The cost matrices P and q look are defined as:

$$P = \begin{bmatrix} R & & & & \\ & Q & & & \\ & & \ddots & & \\ & & & R & \\ & & & & Q \end{bmatrix}, \quad q = \begin{bmatrix} -Ru^{ref} \\ -QT^{ref} \\ \vdots \\ -Ru^{ref} \\ -QT^{ref} \end{bmatrix}$$

This finite-horizon optimal control problem is in line with the form of an SQP problem and is solved using Operator Splitting Quadratic Program (OSQP) [51], a numerical optimization solver for

convex quadratic problems. CVXPY, a Python-embedded modeling language [52] is used in the present work to call the solver.

Appendix D. Resistor–capacitor network model details

For the Resistor-Capacitor (RC) network mentioned in Section 4.1, each zone was represented by an R2C2 room model, where the external wall was modeled by a resistor, two capacitors represented the indoor air and internal mass, and another resistor represented convective heat transfer resistance. Inputs to the model included outdoor temperature T^{OA}, internal heat gains d, HVAC thermal energy input $\mathbf{u}$, and solar irradiance G, with an estimated heat gain coefficient. The internal walls, connecting adjacent zones, were modeled using an R2C1 partition, comprising two resistors and a capacitor. The study modeled external walls with a single resistor, typically for high-performance glass walls with minimal thermal capacitance. Note that if an external wall has a heavy thermal mass, an R2C1 model should be employed. The RC network was built using Modelica. The bounded parameters θ in the RC network were identified by optimizing the following problem:

$$\theta = \arg\min \sum_{k=t_0}^{t_1} \sum_{m=1}^{6} (T_k^m - \overline{T}_k^m)^2$$

$$\text{s.t.} \overline{T}_k^m = f(T_k^{OA}, \mathbf{u}_k, G_k, d_k, \theta)$$

$$\theta_{lb} \le \theta \le \theta_{ub}$$

The identification was defined in Optimica and solved by the interior-point method (IPOPT) using JModelica.

References

[1] National Environment Agency. Climate change - overview. https://www.nea.gov.sg/our-services/climate-change-energy-efficiency/climate-change, Apr. 2023. [Accessed 22 August 2023].

[2] International Energy Agency. Southeast Asia energy outlook 2022. Tech. Rep.. International Energy Agency; May 2022.

[3] International Renewable Energy Agency (IRENA). Statistical profiles. https://www.irena.org/Data/Energy-Profiles, Aug. 2022. [Accessed 22 August 2023].

[4] Quek A, Ee A, Ng A, Wah TY. Challenges in environmental sustainability of renewable energy options in Singapore. Energy Policy 2018;122:388–94.

[5] Lau HC. Decarbonization roadmaps for ASEAN and their implications. Energy Rep 2022;8:6000–22.

[6] Hamilton I, Kennard H, Rapf O, Zuhaib JKS. 2020 global status report for buildings and construction: towards a zero-emission, efficient and resilient buildings and construction sector. Tech. Rep.. United Nations Environment Programme; 2020.

[7] Jensen SØ, Marszal-Pomianowska A, Lollini R, Pasut W, Knotzer A, Engelmann P, et al. IEA EBC annex 67 energy flexible buildings. Energy Build 2017;155:25–34.

[8] Jensen SØ. Energy in buildings and communities programme annex 67 energy flexible buildings. Tech. Rep.. International Energy Agency (IEA); Dec. 2019.

[9] Liu J, Yin R, Yu L, Piette MA, Pritoni M, Casillas A, et al. Defining and applying an electricity demand flexibility benchmarking metrics framework for grid-interactive efficient commercial buildings. Adv Appl Energy 2022;8:100107.

[10] Li H, Wang Z, Hong T, Piette MA. Energy flexibility of residential buildings: a systematic review of characterization and quantification methods and applications. Adv Appl Energy 2021;3:100054.

[11] Li H, Hong T. A semantic ontology for representing and quantifying energy flexibility of buildings. Adv Appl Energy 2022;8:100113.

[12] Airò Farulla G, Tumminia G, Sergi F, Aloisio D, Cellura M, Antonucci V, et al. A review of key performance indicators for building flexibility quantification to support the clean energy transition. Energies 2021;14(18):5676.

[13] Li H, Johra H, de Andrade Pereira F, Hong T, Le Dréau J, Maturo A, et al. Data-driven key performance indicators and datasets for building energy flexibility: a review and perspectives. Appl Energy 2023;343:121217.

[14] Sudhakar K, Winderl M, Priya SS. Net-zero building designs in hot and humid climates: a state-of-art. Case Stud Therm Eng 2019;13:100400.

[15] Afroz Z, Goldsworthy M, White SD. Energy flexibility of commercial buildings for demand response applications in Australia. Energy Build 2023;300:113533.

[16] Troitzsch S, Sreepathi BK, Huynh TP, Moine A, Hanif S, Fonseca J, et al. Optimal electric-distribution-grid planning considering the demand-side flexibility of thermal building systems for a test case in Singapore. Appl Energy 2020;273:114917.

[17] Utama C, Troitzsch S, Thakur J. Demand-side flexibility and demand-side bidding for flexible loads in air-conditioned buildings. Appl Energy 2021;285:116418.

[18] Luthander R, Widén J, Nilsson D, Palm J. Photovoltaic self-consumption in buildings: a review. Appl Energy 2015;142:80–94.

[19] Hanif S, Gruentgens C, Massier T, Hamacher T, Reindl T. Cost-optimal operation for a flexible building with local PV in a Singaporean environment. In: 2016 IEEE power & energy society innovative smart grid technologies conference (ISGT); 2016. p. 1–5.

[20] Zhan S, Dong B, Chong A. Improving energy flexibility and PV self-consumption for a tropical net zero energy office building. Energy Build 2023;278:112606.

[21] Comodi G, Carducci F, Sze JY, Balamurugan N, Romagnoli A. Storing energy for cooling demand management in tropical climates: a techno-economic comparison between different energy storage technologies. Energy 2017;121:676–94.

[22] Energy Authority Market (EMA). Introduction to the national electricity market of Singapore. Tech. Rep.. Energy Authority Market (EMA); 2009.

[23] Samadi P, Mohsenian-Rad A-H, Schober R, Wong VWS, Jatskevich J. Optimal real-time pricing algorithm based on utility maximization for smart grid. In: 2010 first IEEE international conference on smart grid communications; 2010. p. 415–20.

[24] Khan AR, Mahmood A, Safdar A, Khan ZA, Khan NA. Load forecasting, dynamic pricing and DSM in smart grid: a review. Renew Sustain Energy Rev 2016;54:1311–22.

[25] Sheha M, Mohammadi K, Powell K. Solving the duck curve in a smart grid environment using a non-cooperative game theory and dynamic pricing profiles. Energy Convers Manag 2020;220:113102.

[26] Taşcıkaraoğlu A. Economic and operational benefits of energy storage sharing for a neighborhood of prosumers in a dynamic pricing environment. Sustain Cities Soc 2018;38:219–29.

[27] Huang P, Sun Y. A collaborative demand control of nearly zero energy buildings in response to dynamic pricing for performance improvements at cluster level. Energy 2019;174:911–21.

[28] Tang R, Wang S, Li H. Game theory based interactive demand side management responding to dynamic pricing in price-based demand response of smart grids. Appl Energy 2019;250:118–30.

[29] Boiarkin V, Rajarajan M, Al-Zaili J, Asif W. A novel dynamic pricing model for a microgrid of prosumers with photovoltaic systems. Appl Energy 2023;342:121148.

[30] Di Natale L, Svetozarevic B, Heer P, Jones CN. Physically consistent neural networks for building thermal modeling: theory and analysis. Appl Energy 2022;325:119806.

[31] Chen Z, Xiao F, Guo F, Yan J. Interpretable machine learning for building energy management: a state-of-the-art review. Adv Appl Energy 2023;9:100123.

[32] Drgoňa J, Tuor AR, Chandan V, Vrabie DL. Physics-constrained deep learning of multi-zone building thermal dynamics. Energy Build 2021;243:110992.

[33] Gokhale G, Claessens B, Develder C. Physics informed neural networks for control oriented thermal modeling of buildings. Appl Energy 2022;314:118852.

[34] Wang X, Dong B. Physics-informed hierarchical data-driven predictive control for building HVAC systems to achieve energy and health nexus. Energy Build 2023;291:113088.

[35] Chen Y, Yang Q, Chen Z, Yan C, Zeng S, Dai M. Physics-informed neural networks for building thermal modeling and demand response control. Build Environ 2023;234:110149.

[36] Raissi M, Perdikaris P, Karniadakis GE. Physics-informed neural networks: a deep learning framework for solving forward and inverse problems involving nonlinear partial differential equations. J Comput Phys 2019;378:686–707.

[37] Prívara S, Cigler J, Váňa Z, Oldewurtel F, Sagerschnig C, Žáčeková E. Building modeling as a crucial part for building predictive control. Energy Build 2013;56:8–22.

[38] Di Natale L, Svetozarevic B, Heer P, Jones CN. Towards scalable physically consistent neural networks: an application to data-driven multi-zone thermal building models. Appl Energy 2023;340:121071.

[39] Nghiem TX, Drgoňa J, Jones C, Nagy Z, Schwan R, Dey B, et al. Physics-informed machine learning for modeling and control of dynamical systems. In: 2023 American control conference (ACC). IEEE; 2023. p. 3735–50.

[40] Zhang Z, Chong A, Pan Y, Zhang C, Lam KP. Whole building energy model for HVAC optimal control: a practical framework based on deep reinforcement learning. Energy Build 2019;199:472–90.

[41] Yu L, Qin S, Zhang M, Shen C, Jiang T, Guan X. A review of deep reinforcement learning for smart building energy management. IEEE Int Things J 2021;8(15):12046–63.

[42] Drgoňa J, Tuor A, Skomski E, Vasisht S, Vrabie D. Deep learning explicit differentiable predictive control laws for buildings. IFAC-PapersOnLine 2021;54(6):14–9.

[43] Li H, Hong T. On data-driven energy flexibility quantification: a framework and case study. Energy Build 2023;296:113381.

[44] Luthander R, Nilsson AM, Widén J, Åberg M. Graphical analysis of photovoltaic generation and load matching in buildings: a novel way of studying self-consumption and self-sufficiency. Appl Energy 2019;250:748–59.

[45] Xiao T, You F. Building thermal modeling and model predictive control with physically consistent deep learning for decarbonization and energy optimization. Appl Energy 2023;342:121165.

[46] Zhan S, Chong A. Data requirements and performance evaluation of model predictive control in buildings: a modeling perspective. Renew Sustain Energy Rev 2021;142:110835.

[47] Energy Market Company. Nems prices. https://www.nems.emcsg.com/en/nems-prices, Oct. 2023. [Accessed 15 October 2023].

[48] Feng X, Gooi HB, Chen S. Capacity fade-based energy management for lithium-ion batteries used in PV systems. Electr Power Syst Res 2015;129:150–9.

[49] Loi TSA, Ng JL. Analysing households' responsiveness towards socio-economic determinants of residential electricity consumption in Singapore. Energy Policy 2018;112:415–26.
[50] Fuentes M, Nofuentes G, Aguilera J, Talavera DL, Castro M. Application and validation of algebraic methods to predict the behaviour of crystalline silicon PV modules in Mediterranean climates. Sol Energy 2007;81(11):1396–408.
[51] Stellato B, Banjac G, Goulart P, Bemporad A, Boyd S. OSQP: an operator splitting solver for quadratic programs. Math Program Comput 2020;12(4):637–72.
[52] Diamond S, Boyd S. CVXPY: a python-embedded modeling language for convex optimization. J Mach Learn Res 2016;17.